Bull. Mater. Sci. (2022) 45:51
https://doi.org/10.1007/s12034-021-02634-9

Prediction of thermoelectric performance for monolayer HfNI

HUA DAI[1] and BIN XU[2,*]

[1]Zhengzhou Preschool Education College, Zhengzhou 450000, China
[2]North China University of Water Resources and Electric Power, Zhengzhou 450046, China
*Author for correspondence (hnsqxubin@163.com)

MS received 15 July 2021; accepted 14 November 2021

Abstract. The full-potential linearization enhanced plane wave method and the semi-classical Boltzmann theory are used to calculate the thermoelectric properties of monolayer HfNI. For monolayer HfNI, the bandgap, which is calculated by Tran–Blaha-modified Becke–Johnson (TB-mBJ), is larger than that of generalized gradient approximation. There is no imaginary frequency for the phonon band structure of monolayer HfNI, which guarantees its dynamic stability. Although monolayer HfNI has two heavy elements Hf and I atoms, due to the shrinkage effect of lanthanides the phonon gap of monolayer HfNI becomes wide and the phonon dispersion phase space decreases, which suppresses the three-phonon dispersion channel. Moreover, monolayer HfNI has a higher lattice thermal conductivity. Finally, when the carrier concentration is 5×10^{18} cm^{-3}, the ZT_{max} of n-type monolayer HfNI with TB-mBJ is 0.91 at 500 K.

Keywords. Monolayer HfNI; thermoelectric property; electronic structure; Boltzmann transport theory; density functional theory.

1. Introduction

Due to the depletion of fossil fuels and the resulting environmental pollution, exploring sustainable new clean energy has become a global consensus [1]. Thermoelectric (TE) materials can directly convert waste heat into electric energy through temperature difference, which makes carriers in semiconductors emit light, which helps to solve the energy crisis [2–4]. Although TE devices have high reliability and compactness, the relatively low efficiency limits their wide application. Therefore, it is very difficult to find suitable materials with large ZT. In recent years, various types of TE materials have been discovered. For example, skutterudite [5,6], layered cobalt oxide [7,8], half-Heusler alloy [9–11], Zintl compound [12], clathrate [13,14], Bi-Te-Sb family [15,16], two-dimensional (2D) structure of layered materials [17–22], etc. Therefore, it is a great challenge to find high-performance TE materials, and the low-dimensional structure has been used to optimize ZT value [17–22].

Two-dimensional (2D) semiconductors have been widely studied in potential TE applications, because compared with their bulk, low-dimensional structures can significantly improve S and reduce κ [23–30]. The results showed that when T = 210 K, the S-value of 2D blue phosphorus was 510 mV K^{-1}, which was better than 340 mV K^{-1} for bulk phosphorus at 300 K. Wickramaratne *et al* [25] also found a similar phenomenon in Bi_2Te_3 [23,24]. Using first-principles calculations is an effective way to find 2D TE materials with high power factor and low thermal conductivity. For example, Ma *et al* [31] predicted that the metal-coated single-layer 1T-Tl_2O has been proven to be a potential TE material [32]. At the same time, the newly predicted monolayer InP_3 not only shows potential application prospects in photovoltaic solar cells and optoelectronic devices, but also shows good TE performance with ZT as high as 2.06 [33]. In addition, Peng *et al* [26] also discussed the influence of chemical bonds on the electronic and thermal transport properties of anisotropic V-group materials [27].

A large number of TE materials have been discovered in recent decades. A common feature of many high-performance TE materials, such as BiCuSeO, is that many of them have layered crystal structures. As mentioned above, MNX (M = Ti, Zr, Hf; X = Cl, Br) is a material with a layered and anisotropic crystal structure [34–37]. These transition metal nitride halides have easy to adjust electrical transmission properties, and their layered structure usually helps to introduce additional phonon scattering channels through the atomic interaction between layers, so that the materials exhibit inherent low thermal conductivity [38]. This makes MNX compounds a promising candidate for TE devices [39,40].

The current research focuses on the TE properties of HfNCl or ZrNCl. The electron doping in MNCl (M = Hf, Zr) was studied by Weht *et al* [41]. Hotehama *et al* [42] doped layered metal nitride MNCl (M = Zr, Hf) with alkali metal (A = Li, Na) to form AMNCl, and studied its

Published online: 09 March 2022

superconductivity. Akashi *et al* [43] calculated and analysed the density functional theory of superconductors to understand the superconducting mechanism of doped layered nitrides MNCl (M = Ti, Zr and Hf). Since the TE properties of TiNBr have not been systematically studied, we have performed first-principles calculations on the transport properties of TiNBr. This research uses Boltzmann theory and first principles to study and analyse the electronic structure and phonon structure of monolayer HfNI. Our work is to study the TE properties of monolayer HfNI when the carrier concentration range is 5×10^{18} to 5×10^{20} cm^{-3} and the temperature range is 300–600 K.

2. Computational details

Using the full-potential linearized augmented plane wave method as implemented in the WIEN2K code [44], we selected generalized gradient approximation (GGA) and Tran–Blaha modified Becke–Johnson (TB-mBJ) as the exchange-correlation potentials. We consider $R_{mt}K_{ma}$ equal to 9.0 and make the expansion up to l = 10 in the muffin tins spheres. Nonoverlapping muffin tin sphere radii of 2.30, 1.88, and 2.50 a.u. were used for Hf, N and I, respectively. We have used 100000 k-points in the first Brillouin zone. Self-consistency is considered to be finished when the total energy discrepancy between iterations is less than 10^{-5} Ry per formula unit.

According to the semi-classical Boltzmann theory and the rigid band method, we calculated the transport properties of crystalline solids [45]. We use the semi-classical Boltzmann theory to perform transport calculations from electronic structures, as implemented in the BoltzTraP code [46]. The doping is served based on the rigid band approximation [47]. Employing the finite displacement method and the Phonopy package, phonon spectrum is procured by using the $6 \times 6 \times 1$ supercell [48]. We use the phonon Boltzmann transport equation to calculate the lattice thermal conductivity κ_l, which is applied in ShengBTE [49]. The second-order and third-order interatomic force constants for monolayers HfNI are calculated by using a $4 \times 4 \times 1$ supercell with $4 \times 4 \times 1$ k-mesh. We impose a cut-off so as to include interactions up to the eighth nearest neighbours for the third-order interatomic force constants. A cut-off of 0.5 nm for the calculation of harmonic force constants is employed. A denser k-mesh of $37 \times 37 \times 1$ is used to guarantee the convergence of lattice thermal conductivity for monolayer HfNI, which triumphantly forecasted the lattice thermal conductivity [50–53].

3. Results and discussion

Monolayer HfNI is a ternary transition metal nitride, and its space group is R-3m. Hf is a transition metal and also a lanthanide element. Monolayer HfNI consists of six atoms,

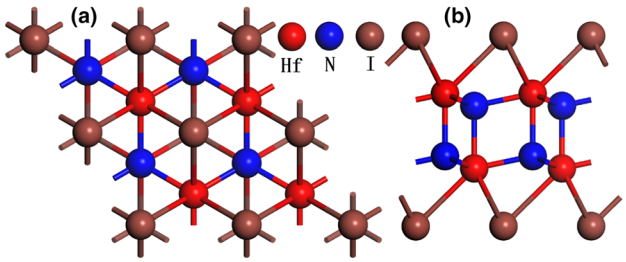

Figure 1. (**a**) Top and (**b**) side views of monolayer HfNI.

which is $(HfNI)_2$. Figure 1 is a top view and a side view of monolayer HfNI. The optimized lattice parameters of monolayer HfNI are $a = b = 3.568$ Å, and $c = 36.669$ Å. Monolayer HfNI is composed of a honeycomb double-layer Hf-N layer sandwiched between the halogen element I layers.

The correct band shape is produced using GGA calculations, but its bandgap will be underestimated. In order to reduce the error, the electronic energy band structure is calculated by the TB-mBJ method [54], and the bandgap is more standard. We used two methods to calculate and analyse the electronic structure of monolayer HfNI. Among them, the electronic structure of TE materials is one of the important factors affecting their performance.

The band structure of monolayer HfNI, the total density and partial density of states are shown in figure 2a, b and c. The maximum valence band of monolayer HfNI obtained by the GGA calculation method is at the Γ point, and the minimum conduction band is at the K point. Therefore, monolayer HfNI has an indirect bandgap (1.322 eV). The energy band structure of monolayer HfNI calculated with TB-mBJ is also an indirect bandgap, but its bandgap is 1.458 eV, which is slightly higher than the result calculated by GGA. In addition, the energy band structure of monolayer HfNCl has the maximum valence band at the Γ point and the minimum conduction band at the K point [55]. But the energy bandgap of monolayer HfNCl is 2.36 eV, in contrast, monolayer HfNI has a lower bandgap.

In terms of the density of states, figure 2c shows the s electronic state, p electronic state and d electronic state. Among the three electronic states, the s state contributes little to the density of states of monolayer HfNI. d state of I and N atoms and p state of Hf atoms also contribute little to the density of states of monolayer HfNI. The density of states of the conduction band is mainly contributed by d state of Hf atoms. The curves of the density of states calculated by GGA and TB-mBJ almost overlap, which shows that their density of states is almost the same. The density of states of the valence band is mainly contributed by p state of the N and I atoms, and a small amount is contributed by d state of Hf atoms. Near the Fermi surface, the density of states is mainly provided by I and N atoms. And the density of states calculated by GGA (especially the density of states contributed by N atoms) is slightly higher than that of TB-mBJ.

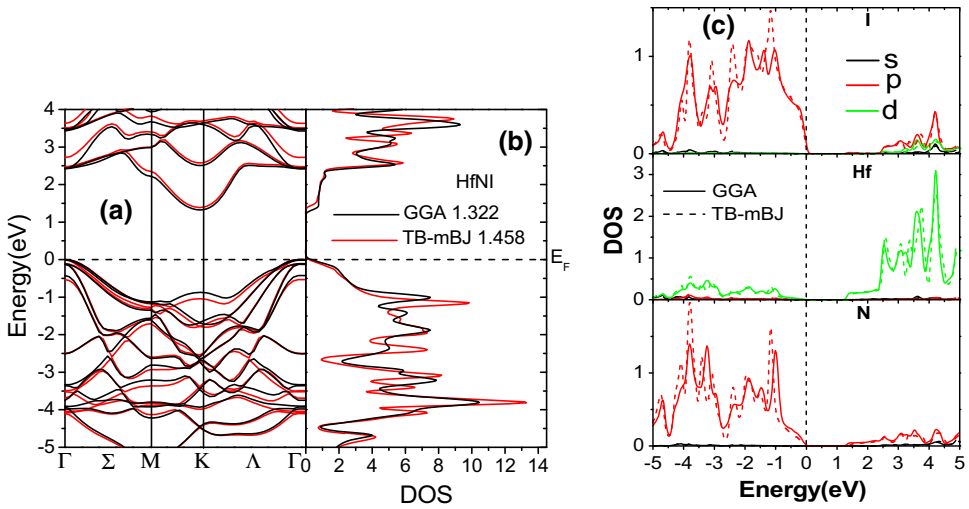

Figure 2. (**a**) Calculated band structures, (**b**) total and (**c**) partial density of states for monolayer HfNI.

The calculated Seebeck coefficient and electrical conductivity of monolayer HfNI as a function of temperature are shown in figure 3a and b when the carrier concentration is 5×10^{18} to 5×10^{20} cm^{-3}. Seebeck coefficient of monolayer HfNI decreases with the increase of carrier concentration and increases with the increase of temperature. At 400 K, Seebeck coefficients are close to p-type and n-type monolayer HfNI calculated with TB-mBJ. The Seebeck coefficient of p-type monolayer HfNI calculated with TB-mBJ at other temperatures is only slightly higher than that of n-type. For example, when the carrier concentration is 5×10^{18} cm^{-3} at 600 K, the Seebeck coefficient of p-type monolayer HfNI calculated with TB-mBJ is about 475 μV K^{-1}, and the Seebeck coefficient of n-type monolayer HfNI is 450 μV K^{-1}. The Seebeck coefficient of p-type monolayer HfNI calculated by GGA is about 515 μV K^{-1}, and the Seebeck coefficient of n-type monolayer HfNI is 445 μV K^{-1}. The S of a good TE material needs to be higher than 200 μV K^{-1} [20]. The Seebeck coefficient of monolayer HfNI is obviously satisfied. We also calculated the average effective mass and relaxation time of monolayer HfNI at 300 K.

As shown in table 1, the Seebeck coefficient is directly proportional to the average effective mass. The average effective mass of electrons and holes is analysed and given in table 1. At 300 K, the average effective mass of the hole calculated by GGA is higher than that of the electron for monolayer HfNI. So the S of p-type HfNI is higher than that

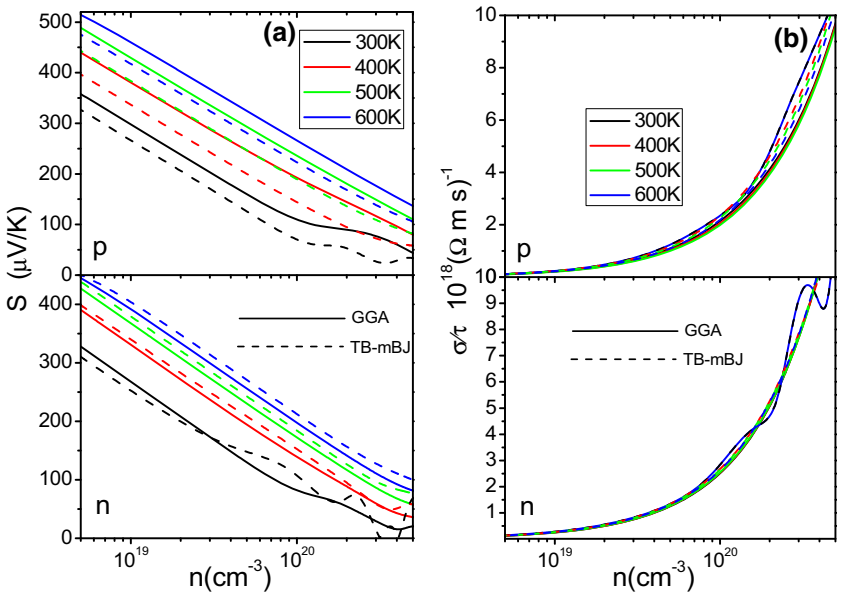

Figure 3. Seebeck coefficient and electrical conductivities as a function of temperature for monolayer HfNI.

Table 1. Calculated deformation potential constant E_l, elastic modulus C_{2D}, effective mass (m^*), average effective mass (m_d), and relaxation time (τ) of electrons and holes for monolayer HfNI at 300 K.

Carrier type	E_1 (eV)	C_{2D} (eV Å^{-2})	m^* (Γ–M) (m_e)	m^* (M–K) (m_e)	m_d (m_e)	τ (10^{-14} s)
Electron (GGA)	7.832	26.538	7.428	0.604	2.119	0.247
Hole (GGA)	12.104	26.538	1.710	16.800	5.361	0.041
Electron (TB-mBJ)	7.832	26.538	2.320	0.549	1.129	0.464
Hole (TB-mBJ)	12.104	26.538	1.786	12.928	4.805	0.259

of n-type for monolayer. The results calculated with TB-mBJ are similar to GGA.

The average effective mass of monolayer HfNI is not only proportional to its Seebeck coefficient, but also inversely proportional to its electrical conductivity. The electrical conductivity is also affected by the relaxation time. The calculation formula is as follows:

$$\sigma = ne\mu \tag{1}$$

$$\mu = \frac{\tau e}{m_d} \tag{2}$$

According to formulas (1) and (2), the electrical conductivity is proportional to the relaxation time. Through calculation, the electrical conductivity of monolayer HfNI as a function of temperature is obtained and shown in figure 3b.

It can be clearly seen from the figure that within the temperature range we calculated, the temperature difference hardly affects the σ/τ value of monolayer HfNI. Especially at 300, 400 and 500 K, the σ/τ curves of n-type monolayer HfNI overlap. When the carrier concentration is 3×10^{20} cm^{-3}, the σ/τ of n-type monolayer HfNI reaches 10×10^{18} $(\Omega ms)^{-1}$. The σ/τ of p-type monolayer HfNI reaches 10×10^{18} $(\Omega ms)^{-1}$ when the carrier concentration is 4×10^{20} cm^{-3}. That is to say, compared with the n-type, with the increase of the carrier concentration, the σ/τ of the p-type monolayer HfNI increases more slowly. Therefore, under the same conditions, the σ/τ of n-type monolayer HfNI is slightly higher than that of p-type. Monolayer HfNI has a low σ/τ. When the carrier concentration is 10^{20} cm^{-3}, σ/τ of monolayer HfNI is only 2×10^{18} $(\Omega ms)^{-1}$. The electrical conductivity is proportional to the TE figure of merit, but it is also proportional to the electronic thermal conductivity. So a lower σ/τ is not necessarily a bad thing.

Next, we will discuss the thermal conductivity of monolayer HfNI. We all know that lower lattice thermal conductivity is critical to the TE properties of the material. Generally speaking, the strong coupling of the acoustic mode and the optical mode, weak atomic bonds and heavy elements will reduce the lattice thermal conductivity κ_l. In particular, κ_l is very sensitive to the mass of heavy elements. Heavy elements will cause low phonon frequencies and low group velocities, which in turn reduces κ_l [56–60]. Both Hf and I atoms are heavier elements. However, the calculated κ_l of monolayer HfNI is much higher than that of Sb_2Te_3/Bi_2Te_3 related alloy materials. κ_l of $AgSbTe_2$ is 0.63 W mK^{-1} [61]. At room temperature, κ_l of Bi_2Te_3 is 1.1 W mK^{-1} [62]. κ_l of SnSe is 0.97 W mK^{-1} [63]. κ_l of PbTe is 1.6 W mK^{-1} [64]. κ_l of Bi_2SeTe_2 is 1.961 W mK^{-1} [65]. To understand the reason for the high κ_l of monolayer HfNI, the phonon spectrum of monolayer HfNI is calculated. The phonon dispersion relationship calculated by monolayer HfNI along the highly symmetrical direction is shown in figure 4a.

It can be seen from figure 4a that the phonon band structure of monolayer HfNI has no imaginary frequency, so its dynamic stability can be guaranteed. In the basic unit lattice, 6 atoms have 18 vibration modes, including three phonon modes (colour lines LA, TA and ZA) and fifteen optical phonon modes.

The maximum frequency of monolayer HfNI is 21.5 THz, which is 716.7 cm^{-1}. This is close to the highest frequency of the phonon spectrum of HfNCl [55], which is 22.36 THz (745.85 cm^{-1}). This is mainly because the mass of I atoms is higher than that of Cl atoms. So the maximum frequency of monolayer HfNI is slightly lower than that of HfNCl. However, the maximum frequencies of the optical modes of Bi_2Te_3 are 136.0, 144.7 and 146.2 cm^{-1} [18,66,67]. The maximum frequency of the photon mode of monolayer Bi_2Te_2Se is 154.1, 152.7 and 154.5 cm^{-1} [65,68,69]. In other words, the maximum frequency of the optical mode of monolayer HfNI is very high. However, κ_l of TE materials exceeding 80% is provided by the acoustic mode. This is because the optical modes are easily scattered. However, the maximum frequency of the acoustic mode of monolayer HfNI is also higher. This is one of the reasons why κ_l of monolayer HfNI is too big, which is a negative effect.

In HfNCl [61], the low-frequency phonons mainly come from Hf and Cl atoms, while the high-frequency optical phonons are mainly contributed by N atoms. It can be seen from figure 4a that there is a wide phonon bandgap from 6 to 12 THz. Figure 4b shows the phonon mode of monolayer HfNI. The modes below the bandgap in the monolayer HfNI phonon spectrum are mainly contributed by Hf and I atoms, and the modes above the bandgap are mainly derived from lighter N atoms. Monolayer HfNI has a wider phononic bandgap because the atoms of monolayer HfNI have a lanthanide shrinkage effect. In other words, monolayer

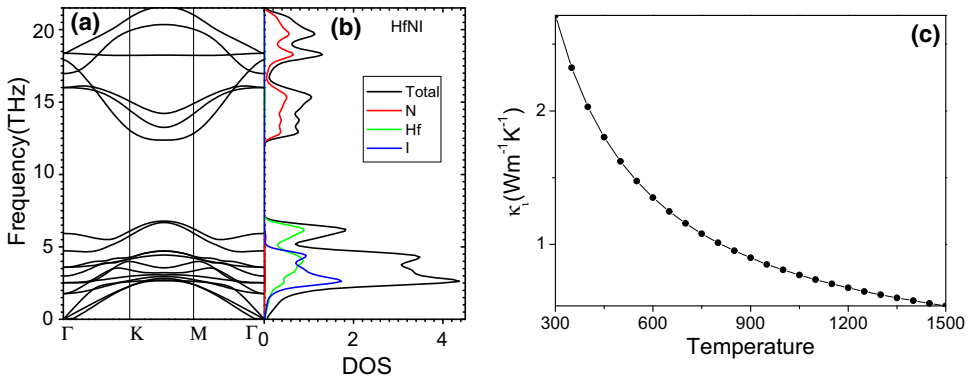

Figure 4. Calculated phonon dispersion relations along high symmetry directions for (**a**) monolayer HfNI and optical modes, respectively; (**b**) density of states of phonon and (**c**) temperature dependence of phonon thermal conductivity.

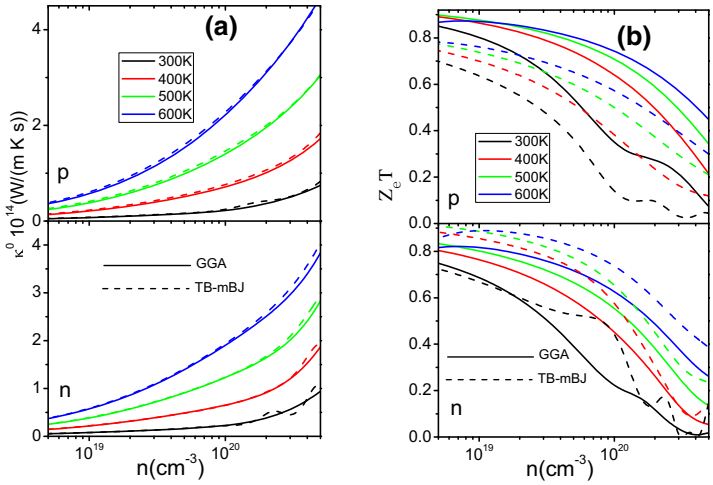

Figure 5. (**a**) Electronic thermal conductivity and (**b**) ZT as a function of temperature for monolayer HfNI.

HfNI has strong Hf-I and Hf-N bonds. This causes the optical branches to move upward and the phonon gap widens. The phase space of phonon dispersion will decrease. This will significantly suppress the three-phonon dispersion channel. κ_l of monolayer HfNI is too big, which is a negative effect.

Therefore, although both Hf and I atoms are heavy elements, monolayer HfNI has a lower group velocity. However, the shrinkage effect of lanthanides surpasses the influence of heavy elements on κ_l. Therefore, κ_l of monolayer HfNI is very high. κ_l of monolayer HfNI as a function of temperature is shown in figure 4b. With the increase of temperature, κ_l of monolayer HfNI gradually decreases. At room temperature, the κ_l of monolayer HfNI is approximately 2.75 W mK^{-1}.

The thermal conductivity is the sum of the lattice thermal conductivity and the electronic thermal conductivity. The electronic thermal conductivity of monolayer HfNI as a function of temperature is shown in figure 5a. Electronic thermal conductivity is mainly affected by electrical conductivity and temperature, and its calculation formula is as follows:

$$\kappa^0 = \frac{L\sigma T}{\tau} \tag{3}$$

The electronic thermal conductivity is directly proportional to temperature and electrical conductivity. Therefore, the electronic thermal conductivity increases with increasing temperature. As the carrier concentration increases, the electronic thermal conductivity of monolayer HfNI increases. Since σ/τ is not high, the electronic thermal conductivity is also not high. Under the same conditions, the electronic thermal conductivity of p-type monolayer HfNI is slightly higher than that of n-type. The electronic thermal conductivity of monolayer HfNI calculated with GGA is slightly lower than that calculated with TB-mBJ.

Although the electronic thermal conductivity of n-type monolayer HfNI is slightly lower than that of p-type, the Seebeck coefficient of n-type monolayer HfNI is also slightly lower than that of p-type. Therefore, the ZT values

of n-type and p-type monolayer HfNI are similar. The TE figure of merit of monolayer HfNI as a function of temperature is shown in figure 5b. Compared with the method of the Cahill model [70], the ShengBTE method [49] estimates the lattice thermal conductivity more accurately. Furthermore, our ZT estimate should be more accurate.

With the increase of carrier concentration, the overall TE figure of merit of monolayer HfNI shows a downward trend. When the carrier concentration is higher than 10^{19} cm^{-3}, the higher the temperature and the greater the TE figure of merit of monolayer HfNI. However, the maximum ZT of both p-type and n-type monolayer HfNI appears when the carrier concentration is 5×10^{18} cm^{-3} and at 500 K.

For p-type monolayer HfNI, ZT calculated by GGA is higher than that calculated by TB-mBJ. This is because the Seebeck coefficient calculated by GGA is higher than that calculated by TB-mBJ. The electrical conductivity and electronic thermal conductivity calculated with GGA are similar to those calculated with TB-mBJ. For n-type monolayer HfNI, except for 300K, ZT calculated with GGA is lower than that calculated with TB-mBJ. ZT calculated by GGA is higher than that calculated by TB-mBJ at 300 K, because the Seebeck coefficient of n-type monolayer HfNI calculated by GGA is only larger at 300 K.

At 500 K and a carrier concentration of 5×10^{18} cm^{-3}, the ZT_{max} of p-type monolayer HfNI calculated by GGA is 0.9. Calculated with a more accurate TB-mBJ, the ZT_{max} of n-type monolayer HfNI is 0.91. Therefore, n-type monolayer HfNI has the largest TE figure of merit when the temperature is 500 K and the carrier concentration is 5×10^{18} cm^{-3}.

4. Conclusions

We use the full-potential linearization enhanced plane wave method and the semi-classical Boltzmann theory to calculate the TE properties of monolayer HfNI. For monolayer HfNI, the bandgap, which is calculated by TB-mBJ, is larger than that of GGA. Monolayer HfNI has an indirect bandgap and two heavy elements—Hf and I atoms. However, due to the shrinkage effect of lanthanides, the phonon gap of monolayer HfNI becomes wider and the phonon dispersion phase space decreases. This suppresses the three-phonon dispersion channel. Monolayer HfNI has a higher lattice thermal conductivity. Finally, when the carrier concentration is 5×10^{18} cm^{-3}, the ZT_{max} of n-type monolayer HfNI calculated with TB-mBJ is 0.91 at 500 K.

Acknowledgements

This research was sponsored by the National Natural Science Foundation of China, under Grant U1404108 and U1804149, and Basic and Frontier Technology Research program of Henan (162300410056).

References

[1] Wang S, SunY Yang J, Duan B, Wu L, Zhang W *et al* 2016 *Energ. Environ. Sci.* **9** 3436
[2] Feng Z, Zhang J, Yan Y, Zhang G, Wang C, Peng C *et al* 2017 *Sci. Rep.* **7** 2572
[3] Shi X, Yang J, Salvador J R, Chi M, Cho J Y, Wang H *et al* 2011 *J. Am. Chem. Soc.* **133** 7837
[4] Tritt T M 1999 *Science* **283** 804
[5] Dahal T, Jie Q, Lan Y C, Guo C F and Ren Z F 2014 *Phys. Chem. Chem. Phys.* **16** 18170
[6] Mallick M M and Vitta S 2017 *Inorg. Chem.* **56** 5827
[7] Chen S D, He Y, Zong A, Zhang Y, Hashimoto M, Zhang B B *et al* 2017 *Phys. Rev. B* **96** 081109
[8] Vikram and Kangsabanik J 2017 *J. Mater. Chem. A* **5** 6131
[9] Xu B, Zhang J, Li X F, Yu G Q, Ma S S, Wang Y S *et al* 2014 *Mater. Res. Innov.* **18** 104
[10] Xu B, Long C G, Wang Y S and Yi L 2012 *Chem. Phys. Lett.* **529** 45
[11] Shuai J, Wang Y M, Kim H S, Liu Z H, Sun J Y, Chen S *et al* 2015 *Acta Mater.* **93** 187
[12] Sui F, He H, Bobev S, Zhao J, Osterloh F E and Kauzlarich S M 2015 *Chem. Mater.* **27** 2812
[13] Yan X L, Ikeda M, Zhang L, Bauer E, Rogl P, Giester G *et al* 2018 *J. Mater. Chem. A* **6** 1727
[14] Tan M, Hao Y M, Yuan D and Chen J Y 2018 *Appl. Surf. Sci.* **443** 11
[15] Choi H, Kim S J, Kim Y J, We J H, Oh M W and Cho B J 2017 *J. Mater. Chem. C* **5** 8559
[16] Mehta R J, Zhang Y, Zhu H, Parker D S, Belley M, Singh D J *et al* 2012 *Nano Lett.* **12** 4523
[17] Shafique A, Samad A and Shin Y H 2017 *Phys. Chem. Chem. Phys.* **19** 20677
[18] Qin D, Ge X J, Ding G Q, Gao G Y and Lv J T 2017 *RSC Adv.* **7** 47243
[19] Ding G Q, Gao G Y, Huang Z S, Zhang W X and Yao K L 2016 *Nanotechnology* **27** 375703
[20] Zhang Z, Chen P, Duan X, Zang K, Luo J and Duan X 2017 *Science* **357** 788
[21] Ding G Q, Wang C, Gao G Y, Yao K L, Dun C C, Feng C B *et al* 2018 *Nanoscale* **10** 7077
[22] Xu B, Zhang J, Yu G Q, Ma S S, Wang Y S and Wang Y X 2018 *J. Appl. Phys.* **124** 165104
[23] Zahid F and Lake R 2010 *Appl. Phys. Lett.* **97** 212102
[24] Maassen J and Lundstrom M 2013 *Appl. Phys. Lett.* **102** 093103
[25] Wickramaratne D, Zahid F and Lake R K 2015 *J. Appl. Phys.* **118** 075101
[26] Peng B, Zhang H, Shao H, Xu K, Ni G, Li J and Soukoulis C M 2018 *J. Mater. Chem. A* **6** 2018
[27] Hsu K F, Loo S, Guo F, Chen W, Dyck J S, Uher C *et al* 2004 *Science* **303** 818
[28] Biswas K, He J Q, Blum I D, Wu C, Hogan T P, Seidman D N *et al* 2012 *Nature* **489** 414
[29] Poudel B, Hao Q, Ma Y, Lan Y C, Minnich A, Yu B *et al* 2008 *Science* **320** 634
[30] Wickramaratne D, Zahid F and Lake R K 2014 *J. Chem. Phys.* **140** 124710
[31] Ma Y, Kuc A and Heine T 2017 *J. Am. Chem. Soc.* **139** 11694
[32] Huang H H, Xing G, Fan X, Singh D J and Zheng W T 2019 *J. Mater. Chem. C* **7** 5094

[33] Ouyang T, Jiang E, Tang C, Li J, He C and Zhong J 2018 *J. Mater. Chem. A* **6** 21532
[34] Zhang S, Tanaka M, Zhu H and Yamanaka S 2013 *Supercond. Sci. Technol.* **26** 085015
[35] Zhang S, Tanaka M, Watanabe E, Zhu H, Inumaru K and Yamanaka S 2013 *Supercond. Sci. Technol.* **26** 122001
[36] Saito Y, Kasahara Y, Ye J, Iwasa Y and Nojima T 2015 *Science* **350** 409
[37] Harshman D R and Fiory A T 2015 *J. Supercond. Nov. Magn.* **28** 2967
[38] Snyder G J and Toberer E S 2008 *Nat. Mater.* **7** 105
[39] Zhang S, Xu B, Lin Y, Nanc C and Liu W 2019 *RSC Adv.* **9** 12886
[40] Wang C and Gao G Y 2020 *J. Phys: Condens. Matter.* **32** 205503
[41] Weht R, Filippetti A and Pickett W E 1999 *Europhys. Lett.* **48** 320
[42] Hotehama K I, Koiwasaki T, Umemoto K, Yamanaka S and Tou H 2010 *J. Phys. Soc. Jpn.* **79** 014707
[43] Akashi R, Nakamura K, Arita R and Imada M 2012 *Phys. Rev. B* **86** 054513
[44] Blaha P, Schwarz K, Madsen G K H, Kvasnicka D and Luitz J 2002 *Computer Code WIEN2K* (Vienna University of Technology, 2002) *Improved, updated Unix version of the original* Blaha P, Schwarz K, Sorantin P and Trickey S B 1990 *Comput. Phys. Commun.* **59** 399
[45] Allen P B 1996 in Chelikowsky J R, Louie S G (eds) *Quantum theory of real materials* (Klüwer, Boston) p 219
[46] Madsen G K H and Singh D J 2006 *Comput. Phys. Commun.* **175** 67
[47] Pfitzner A 1994 *Z. Krist. Cryst. Mater.* **209** 685
[48] Togo A, Oba F and Tanaka I 2008 *Phys. Rev. B* **78** 134106
[49] Li W, Carrete J, Katcho N A and Mingo N 2014 *Comput. Phys. Commun.* **185** 1747
[50] Zhao T Q, Sun Y J, Shuai Z G and Wang D 2017 *Chem. Mater.* **29** 6261
[51] Ding G Q, Gao G Y, Yu L, Ni Y and Yao K L 2016 *J. Appl. Phys.* **119** 025105
[52] Ding G Q, Chen J F, Yao K L and Gao G Y 2017 *New J. Phys.* **19** 073036
[53] Li G P, Ding G Q and Gao G Y 2017 *J. Phys. Condens. Matter* **29** 015001
[54] Tran F and Blaha P 2009 *Phys. Rev. Lett.* **102** 226401
[55] Yun W S and Lee J D 2017 *Sci. Rep.* **7** 17330
[56] Shen J J, Fang T, Fu T Z, Xin J Z, Zhao X B and Zhu T J 2019 *J. Inorg. Mater.* **34** 260
[57] Liu P F, Bo T, Xu J, Yin W, Zhang J, Wang F *et al* 2018 *Phys. Rev. B* **98** 235426
[58] Fang C M, Groot R A and Wiegers G A 2002 *J. Phys. Chem. Solids* **63** 457
[59] Saha S K 2015 *Phys. Rev. B* **92** 041202
[60] Pei Y, Chang C, Wang Z, Yin M, Wu M, Tan G *et al* 2016 *J. Am. Chem. Soc.* **138** 16364
[61] Zhang S N, Zhu T J and Yang S H 2010 *Acta Mater.* **58** 4160
[62] Qiu B and Ruan X 2009 *Phys. Rev. B* **80** 165203
[63] Carrete J, Mingo N and Curtarolo S 2014 *Appl. Phys. Lett.* **105** 101907
[64] Pei Y L and Liu Y 2012 *J. Alloys Compd.* **514** 40
[65] Xu B, Song L G, Peng G H and Zhang J 2019 *Phys. Lett. A* **383** 125864
[66] Chis V, Sklyadneva I Y, Kokh K A, Volodin V A, Tereshchenko O E and Chulkov E V 2012 *Phys. Rev. B* **86** 174304
[67] Zhang J, Liu H J, Cheng L, Wei J, Shi J, Tang X F and Uher C 2014 *J. Appl. Phys.* **116** 023706
[68] Wang B, Niu X N, Ouyang Y X, Zhou Q H and Wang J L 2018 *J. Phys. Chem. Lett.* **9** 487
[69] Rusinov I P, Nechaev I A and Chulkov E V 2013 *J. Exp. Theor. Phys. Lett.* **116** 1006
[70] Cahill D G, Watson S K and Pohl R O 1992 *Phys. Rev. B* **46** 6131